

A spectrally enriched AMR prolongation operator for hybrid LES-DNS of phase interfaces

By N. R. Thakkar[†] AND M. Herrmann[†]

Direct numerical simulations (DNS) of two-phase flow applications such as atomization are prohibitively expensive since there is a need to not only resolve the smallest turbulence scales, but also the smallest capillary and atomization scales. Large eddy simulations (LES) on the other hand, address this limitation by modeling these scales from knowledge of larger scales. While well-established and validated models exist for LES of single-phase flows, there is a lack of general sub-grid closure models for multi-phase flows. Typically, in LES of turbulent two-phase flows involving immiscible fluids, unclosed terms such as those due to the discontinuous change of material properties at the phase interface and surface tension are either outright ignored or treated in a simplified way. An alternative to avoid the closure problem altogether is to use adaptive mesh refinement (AMR) with a high-resolution DNS mesh in the vicinity of the phase interface and aggressively coarsened meshes with standard single-phase LES models elsewhere. The resulting closure problem is then reduced to two standard single-phase sub-grid momentum flux closures. However, even in single-phase flows, LES with abrupt mesh resolution changes, the inherent feature of AMR, are known to suffer from several shortcomings, among them filter commutation errors, energy pile-up in fine-to-coarse mesh transitions and a slow fill-in of small scales in coarse-to-fine mesh transitions (Piomelli *et al.* 2006). The present study aims to address the latter issue by proposing a spectrally enriched AMR prolongation operator based on the differential filtering technique of Bassenne *et al.* (2019). The approach helps recover the resolvable small scales upon mesh refinement by injecting an appropriate amount of energy into the newly resolved scales. The resulting spectrally enriched AMR hybrid LES-DNS is verified using curvature statistics of DNS of normal propagating interfaces placed in decaying homogeneous isotropic turbulence.

1. Introduction

In nature and numerous engineering applications, phase interfaces in turbulent flows play an important role, e.g., atomization processes in engines or medical spray devices, or mixing processes in breaking waves. In engine chambers, for example, the ability to accurately and efficiently simulate the atomization process, i.e., the generation of a spray consisting of small-scale droplets from a bulk liquid, can lead to significant improvements in fuel efficiency and engine emissions.

DNS can explore the underlying physics of atomization from the first principle, necessitating resolving the smallest turbulence, capillary, and atomization scales. However, such DNS is computationally extremely expensive since applications span several orders of length and time scales. Thus, many DNSs are limited to relatively small Reynolds and Weber numbers to limit the range of scales involved. LES, on the other hand, models the smallest scales and thus is potentially significantly less expensive than DNS.

[†] School for Engineering of Matter, Transport and Energy, Arizona State University

Some LES models for turbulent two-phase flows with immiscible fluids have been proposed (Labourasse *et al.* 2007; Toutant *et al.* 2008; Chesnel *et al.* 2011; Shirani *et al.* 2011; Liovic & Lakehal 2012; Grosshans 2013; Aniszewski 2016; Saeedipour & Schneiderbauer 2021; Hasslberger *et al.* 2020; Meller *et al.* 2022). A conjecture exists within these LES approaches that the small unresolved scales can be inferred from the dynamics of the interface on the large, resolved scales. While generally effective for turbulent single-phase flows due to the existence of an energy cascade, whether a similar cascade exists for phase interfaces in turbulent flows is an open question.

It is known that viscosity acts as a dissipative mechanism in turbulent flows at the smallest scales. For phase interfaces, surface tension is thought to play a similar role as viscosity, acting as a dissipative mechanism to prevent the generation of small scale corrugations, resulting in the concept of Kolmogorov's critical radius (Kolmogorov 1949), also known as the Hinze scale (Hinze 1955). However, this depends on the local shape of the phase interface. Kolmogorov's critical radius assumes the phase interface to be spherical in shape. Thus, corrugations induced onto the surface by turbulent eddies have to overcome the restorative effect of the surface tension forces. Similar arguments hold for locally flat phase interfaces. However, if the phase interface is locally in a cylindrical shape, for instance, a ligament, then corrugations introduced by turbulent eddies can be enhanced due to the Rayleigh-Plateau instability. Which effect of surface tension is locally in play therefore depends on the local, i.e., small-scale phase interface geometry. Since the generation of droplets in most atomizers occurs predominantly via the breakup of ligaments (Marmottant & Villermaux 2004), LES closure models for surface tension based on Kolmogorov's critical radius are questionable. A general LES closure model for surface tension thus should account for the local sub-filter geometry of the phase interface, a concept that runs counter to the traditional LES modeling approach based on inferring the physics of the sub-filter scale solely from the resolved scale information.

Some LES closure models have been proposed that suggest maintaining an embedded DNS scale phase interface within an LES scale mesh (Herrmann & Gorokhovski 2008; Herrmann *et al.* 2018; Goodrich *et al.* 2022). While notably cheaper in computational cost than DNS's, such dual-scale LES approaches still are comparatively expensive.

An approach to avoid the closure problem altogether while still retaining most of the computational efficiency of the LES approach is to use AMR. Consider a mesh that is aggressively refined from a typical LES mesh resolution away from the phase interface in the single-phase regions of the flow to a DNS scale resolution at the phase interface. If the region of DNS resolution that contains the phase interface is maintained large enough such that no LES filter operation contains the interface, then the closure problem reduces to two single-phase closures for the sub-filter momentum flux term: one in the liquid and one in the gas. To be computationally tractable, this hybrid LES-DNS approach requires aggressive dynamic mesh refinement and coarsening away from the phase interface with band sizes for a resolution level of typically only one to four cells (Li & Soteriou 2018; Kuo & Trujillo 2018; Chang *et al.* 2022; Zhang *et al.* 2020).

However, sudden changes in mesh resolution, i.e., sudden changes in LES filter sizes, result in several challenges for LES modeling, even in single-phase flows (Kravchenko 1996; Cook 1999; Piomelli *et al.* 2006; and Vanella *et al.* 2008). These include filter commutation errors, small-scale energy pileup at fine-to-coarse mesh transitions and a lack of small-scale eddies after coarse-to-fine mesh transitions that take long to self-generate. Hybrid AMR LES-DNS of turbulent atomization is subject to all of these shortcomings. For example, the high Reynolds and Weber number atomization simulations by Chang

et al. (2022) show an abnormally smooth phase interface lacking expected small-scale interface corrugations. We postulate that this is due to an unphysical lack of small-scale, mesh-resolvable, turbulent eddies after coarse-to-fine mesh transitions.

The present study addresses this shortcoming by proposing an enhanced prolongation operator when cells undergo mesh refinement due to the movement of the phase interface. The operator combines the spectral differential filtering procedure of Bassenne *et al.* (2019) with a traditional gradient-based mesh refinement operator (Popinet 2003). To verify the new operator, hybrid AMR LES-DNS of normal propagating interfaces between immiscible fluids of equal density and viscosity in decaying HIT are compared to DNS results, focusing on the resulting interfacial curvature statistics, since the probability density function (PDF) of curvature is considered to be a pre-cursor metric for the resulting droplet size distribution if the interface undergoes atomization (Zandian *et al.* 2019).

2. Governing equations

The governing equations for the unsteady flow of two immiscible fluids in the incompressible limit are given as,

$$\nabla \cdot \mathbf{u} = 0 \quad (2.1)$$

$$\frac{\partial \rho \mathbf{u}}{\partial t} + \nabla \cdot (\rho \mathbf{u} \otimes \mathbf{u}) = -\nabla p + \nabla \cdot (\mu(\nabla \mathbf{u} + \nabla^T \mathbf{u})) + \sigma \kappa \delta(\mathbf{x} - \mathbf{x}_f) \mathbf{n}. \quad (2.2)$$

Here, \mathbf{u} is the velocity vector, p is the pressure, ρ is the density, μ is the dynamic viscosity, σ is the surface tension coefficient, κ is the interface curvature, δ is the Dirac delta function, \mathbf{n} is the interface unit normal vector and \mathbf{x}_f is the location of the phase interface separating the two fluids.

The motion of a phase interface with normal propagation can be described by

$$\frac{\partial \psi}{\partial t} + (\mathbf{u} + s_L \mathbf{n}) \cdot \nabla \psi = 0. \quad (2.3)$$

Here, ψ is the liquid volume fraction and s_L is the normal propagation speed of the interface. Applying a spatial filter $\bar{\cdot}$ with an assumption that the filter commutes for spatial and temporal derivatives, both Eqs. (2.1) and (2.2) then become

$$\nabla \cdot \bar{\mathbf{u}} = 0 \quad (2.4)$$

$$\frac{\partial \bar{\rho} \bar{\mathbf{u}}}{\partial t} + \nabla \cdot (\bar{\rho} \bar{\mathbf{u}} \otimes \bar{\mathbf{u}}) = -\nabla \bar{p} + \nabla \cdot (\bar{\mu}(\nabla \bar{\mathbf{u}} + \nabla^T \bar{\mathbf{u}})) + \bar{\mathbf{T}}_\sigma + \boldsymbol{\tau}_1 + \nabla \cdot (\boldsymbol{\tau}_2 + \boldsymbol{\tau}_3), \quad (2.5)$$

where the unclosed sub-filter terms are due to surface tension, $\bar{\mathbf{T}}_\sigma$, acceleration, $\boldsymbol{\tau}_1$, momentum transport, $\boldsymbol{\tau}_2$, and viscous effects, $\boldsymbol{\tau}_3$,

$$\bar{\mathbf{T}}_\sigma = \overline{\sigma \kappa \delta(\mathbf{x} - \mathbf{x}_f) \mathbf{n}} \quad (2.6)$$

$$\boldsymbol{\tau}_1 = \frac{\partial \bar{\rho} \bar{\mathbf{u}}}{\partial t} - \overline{\frac{\partial \rho \mathbf{u}}{\partial t}} \quad (2.7)$$

$$\boldsymbol{\tau}_2 = \overline{\rho \mathbf{u} \otimes \mathbf{u}} - \bar{\rho} \bar{\mathbf{u}} \otimes \bar{\mathbf{u}} \quad (2.8)$$

$$\boldsymbol{\tau}_3 = \overline{\mu(\nabla \mathbf{u} + \nabla^T \mathbf{u})} - \bar{\mu}(\nabla \bar{\mathbf{u}} + \nabla^T \bar{\mathbf{u}}) \quad (2.9)$$

Applying a spatial filter to the VoF transport equation, Eq. (2.3), gives

$$\frac{\partial \bar{\psi}}{\partial t} + \nabla \cdot (\bar{\mathbf{u}} + \overline{s_L \mathbf{n}}) \bar{\psi} = \bar{\psi} \nabla \cdot (\bar{\mathbf{u}} + \overline{s_L \mathbf{n}}) + \nabla \cdot \boldsymbol{\tau}_\psi + \boldsymbol{\tau}_4. \quad (2.10)$$

Here, $\boldsymbol{\tau}_4$ is the sub-filter interfacial transport term,

$$\boldsymbol{\tau}_4 = (\overline{\mathbf{u} + \mathbf{s}_L \mathbf{n}}) \overline{\psi} - \overline{(\mathbf{u} + \mathbf{s}_L \mathbf{n}) \psi}. \quad (2.11)$$

3. The hybrid AMR LES-DNS approach

In the present hybrid AMR LES-DNS approach, the extension of the DNS scale mesh containing the phase interface is chosen large enough to guarantee that all spatial filters of the LES scale mesh levels, i.e., the meshes coarser than the DNS mesh, do not contain any part of the phase interface or a non-zero value of the numerical delta function in Eq. (2.6). Then, on the LES scale meshes, $\overline{\rho} = \rho$, $\overline{\mu} = \mu$, $\overline{\delta} = 0$, $\overline{\psi} = 0$ or 1, and thus $\overline{\mathbf{T}}_\sigma = 0$, $\boldsymbol{\tau}_1 = 0$, $\boldsymbol{\tau}_3 = 0$ and $\boldsymbol{\tau}_4 = 0$. The only remaining term requiring closure is $\boldsymbol{\tau}_2$, Eq. (2.8). Thus, the filtered governing equations are simply

$$\nabla \cdot \overline{\mathbf{u}} = 0 \quad (3.1)$$

$$\frac{\partial \overline{\mathbf{u}}}{\partial t} + \nabla \cdot (\overline{\mathbf{u}} \otimes \overline{\mathbf{u}}) = -\frac{1}{\rho} \nabla \overline{p} + \nu \nabla \cdot ((\nabla \overline{\mathbf{u}} + \nabla^T \overline{\mathbf{u}})) + \nabla \cdot \boldsymbol{\tau}_2. \quad (3.2)$$

Since ρ is constant in either fluid, $\boldsymbol{\tau}_2$ can be closed using standard single-phase LES closure models, for example, the dynamic Smagorinsky eddy viscosity model (Germano *et al.* 1991). No filtered equation for the volume fraction ψ , Eq. (2.10), needs to be solved since, by definition, $\overline{\psi} = 0$ and 1 in the gas and in the liquid, respectively.

On the DNS scale mesh containing the phase interface, Eqs. (2.2) and (2.3) are solved, requiring no further closure models. Note that due to the successive refinement of the mesh in bands surrounding the DNS scale mesh, the contribution of the sub-filter momentum flux $\boldsymbol{\tau}_2$ successively vanishes until it theoretically disappears on the DNS scale mesh. Thus, one can solve either Eq. (2.2) or (3.2) on the DNS scale mesh. The former favors computational efficiency, while the latter (used here) favors implementation simplicity.

3.1. Spectral differential filtered prolongation operator

In standard AMR, upon mesh refinement, solution variables in newly refined cells of size Δ are calculated using a prolongation operator, for example, the gradient-based prolongation operator of Popinet (2003),

$$v(\varphi) = v(\chi) + d_x \nabla_x v(\chi) + d_y \nabla_y v(\chi) + d_z \nabla_z v(\chi). \quad (3.3)$$

Here, using the terminology of Popinet (2003), v represents the quantity of interest, χ and φ represent the coarse and newly refined fine cells, respectively, and d represents the relative distance between the coarse and fine cell centers.

In the spectral differential filtered (SDF) prolongation operator, we follow the procedure introduced by Bassenne *et al.* (2019) for reconstructing subgrid scale velocities. Before applying the standard prolongation operator, Eq. (3.3), an approximate deconvolution operator is applied to the velocity field on the to-be-refined coarse mesh cell of size 2Δ .

$$u_{i,AD}^{(2\Delta)} = u_i^{(2\Delta)} - \frac{\partial}{\partial x_j} \left[b^2 \frac{\partial u_i^{(2\Delta)}}{\partial x_j} \right]. \quad (3.4)$$

Next, the prolongation operator, Eq. (3.3), is applied to $u_{i,AD}^{(2\Delta)}$, resulting in $u_{i,ADI}^{(\Delta)}$. Then,

the newly resolvable velocity fluctuations $u_{i,SGS}^{(\Delta)}$ are reconstructed as

$$u_{i,SGS}^{(\Delta)} = \sqrt{2K} \frac{D_i}{\sqrt{D_j D_j}}, \quad (3.5)$$

where, K represents the local sub-grid-scale (SGS) kinetic energy, modeled as

$$K = \frac{\mathcal{C}}{2} \left(u_{i,AD}^{(2\Delta)} - \widetilde{u_{i,AD}^{(2\Delta)}} \right) \left(u_{i,AD}^{(2\Delta)} - \widetilde{u_{i,AD}^{(2\Delta)}} \right), \quad (3.6)$$

with $\mathcal{C} = 0.63$. D_i is an estimate of the local instantaneous growth-rate vector, modeled as

$$D_i = N_i - \widetilde{N}_i \quad (3.7)$$

with

$$N_i = \left[u_{j,ADI}^{(\Delta)} - \widetilde{u_{j,ADI}^{(\Delta)}} \right] \frac{\partial u_{i,ADI}^{(\Delta)}}{\partial x_j}. \quad (3.8)$$

In the above equations, $\widetilde{(\cdot)}$ denotes a spatial filter with characteristic width 4Δ . Finally, an additional approximate deconvolution is applied to obtain the velocity on the refined mesh.

$$u_i^{(\Delta)} = \left(u_{i,ADI}^{(\Delta)} + u_{i,SGS}^{(\Delta)} \right) - \frac{\partial}{\partial x_j} \left[\frac{b^2}{4} \frac{\partial}{\partial x_j} \left(u_{i,ADI}^{(\Delta)} + u_{i,SGS}^{(\Delta)} \right) \right]. \quad (3.9)$$

4. Numerical method

Both the filtered and unfiltered governing equations are solved using a collocated, unstructured, kinetic energy preserving, second-order finite volume fractional step flow solver based on the Cartesian AMR framework FARCOT of Ballesteros (2019). Aggressive refinement is maintained to favor a tractable computational cost by using a constant band size of four cells in each Cartesian direction between each mesh transition boundary. The mesh refinement criterion is based on the location of the phase interface using a fast marching method to ensure the desired band size for each resolution level.

Equation (2.3) is solved using the three-dimensional unsplit geometric VoF method of Owkes & Desjardins (2014) within the refined local surface grid framework (Herrmann 2008). The curvature is calculated using the height function method of Popinet (2009).

In order to maintain the mean interface position of the normal propagating interface, a Galilean transformation is applied, with the transformation velocity increment Δv_y calculated from the motion of the mean interface position

$$\Delta v_y = \frac{d}{dt} y_{\langle \psi \rangle = 0.5}. \quad (4.1)$$

Here, angular brackets $\langle \cdot \rangle$ denote planar averages in the mean interface normal direction, and the mean interface position is defined as the location y where $\langle \psi \rangle = 0.5$.

Instead of applying the Galilean velocity globally to the velocity field \mathbf{u} , here, it is applied directly to Eq. (2.3).

$$\frac{\partial \psi}{\partial t} + (\mathbf{u} + s_L \mathbf{n} - v_y e_y) \cdot \nabla \psi = 0, \quad (4.2)$$

with e_y the unit normal of the mean interface. This approach minimizes the mean momentum transport through mesh refinement boundaries. In fact, one can control the

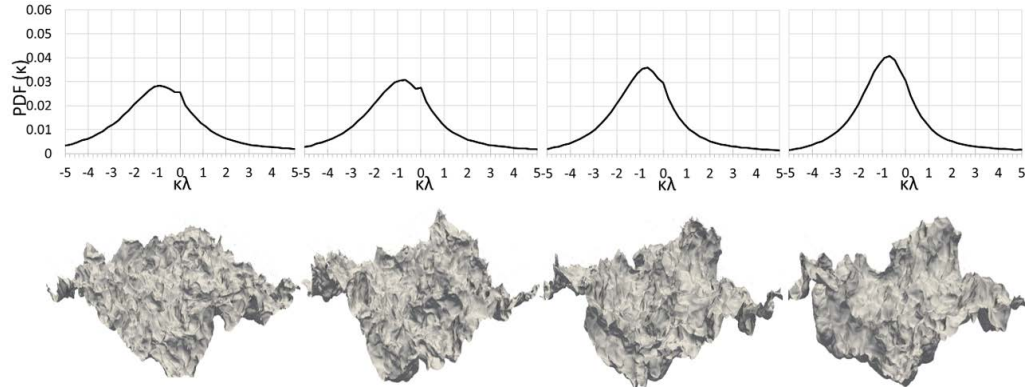


Figure 1. DNS curvature PDF (top) and phase interface geometry (bottom) for $s_L/u' = 0.85$ at time $t/t_L = 0.25, 0.5, 0.75,$ and 1 (from left to right).

amount of momentum transport through the mesh refinement boundaries by adding a constant velocity $v_m e_y$ to \mathbf{u} . However, to focus on the effect of prolongation during mesh refinement, v_m is chosen as $v_m = 0$ here.

5. Results and discussion

5.1. Initial conditions and parameters

A planar interface with y direction normal is placed inside a 2π triply periodic box of decaying HIT with an initial Reynolds number of $Re_\lambda = 162$ (Chiodi & Desjardins 2017). The interface has a constant normal propagation speed of $s_L/u' = 0.85$, where u' is the RMS of the initial turbulent velocity field. No surface tension is considered, i.e., $\sigma = 0$, and the fluids have unit density and viscosity ratios.

5.2. DNS reference results

As a reference solution for verification of the SDF prolongation operator, DNS using a uniform mesh of 512^3 cells is used. As the relevant comparison metric, the surface-area-weighted PDF of the phase interface curvature κ is chosen, since the interfacial curvature statistics are related to the drop size distribution resulting from atomization (Zandian *et al.* 2019). Figure 1 shows the PDF of curvature at different instances in time up to one eddy turn over time t_L .

The PDF exhibits an asymmetry due to Huygen’s principle of normal propagating interfaces, i.e., concave regions of gas penetrating the liquid ($\kappa < 0$) will flatten and convex regions of liquid penetrating the gas ($\kappa > 0$) will form cusps, as seen in interface geometry shown in Figure 1. Kinematic restoration (Peters 1992) limits the generation of high curvature regions. Thus, the normal propagation, in essence, acts similar to surface tension at Kolmogorov’s critical radius (Hinze scale), albeit at the Gibson scale. Note that the kink seen near $\kappa\lambda = 0$ at early times is likely a statistical artifact that would require ensemble averaging to eliminate.

5.3. LES-DNS with standard prolongation operator

The hybrid AMR LES-DNS is initialized with a DNS scale mesh of width $\alpha = 4$ cells in each direction of the initially planar interface, progressively coarsened in bands of α cells

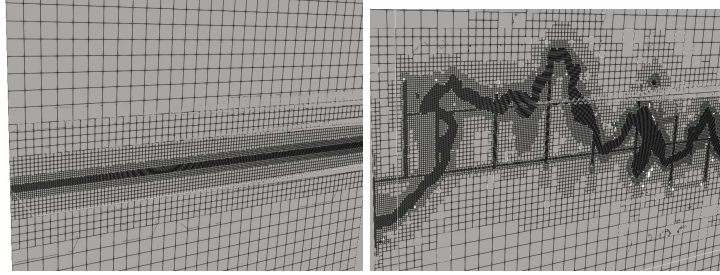


Figure 2. AMR LES-DNS mesh snapshot at $t/t_L = 0$ (left) and 0.5 (right).

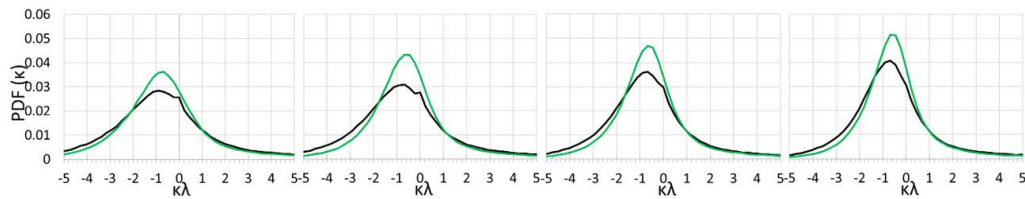


Figure 3. PDF of interfacial curvature at $t/t_L = 0.25, 0.5, 0.75,$ and 1 (left to right) for $s_L/u' = 0.85$ from DNS (black) and LES-DNS with standard prolongation (green).

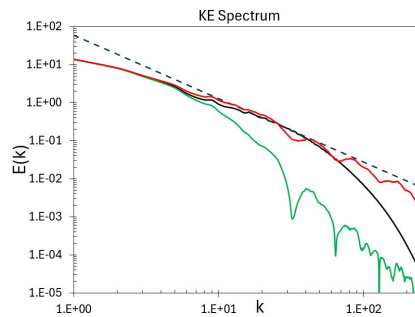


Figure 4. Initial kinetic energy spectrum: DNS (black), AMR LES-DNS with standard prolongation (green), AMR-LES with SDF prolongation (red), and $-5/3$ (dashed).

to the LES resolution of 32^3 cells, as shown in Figure 2 (left). On each mesh level, the velocity is initialized to the appropriately filtered initial DNS scale velocity. The mesh dynamically evolves and is updated every time step as shown in Figure 2 (right).

Figure 3 shows the PDF of curvature when using a standard gradient-based prolongation operator for newly refined cells. Clearly, the standard operator under-predicts the probability of finding high-curvature regions and thereby over-predicts the probability of finding low-curvature regions. The lack of high curvature regions indicates a lack of small-scale eddies that could corrugate the interface at small scales. This is indeed the case as the following experiment demonstrates.

Consider as a starting point the initial velocity field of the LES-DNS on the LES mesh scale of 32^3 . For that fluid to reach the phase interface, it has to undergo multiple mesh refinement steps applying the standard prolongation operator until reaching the DNS scale mesh of 512^3 . To mimic this process, Figure 4 shows the kinetic energy spectrum of the initial LES scale velocity field, successively refined to the DNS scale using the

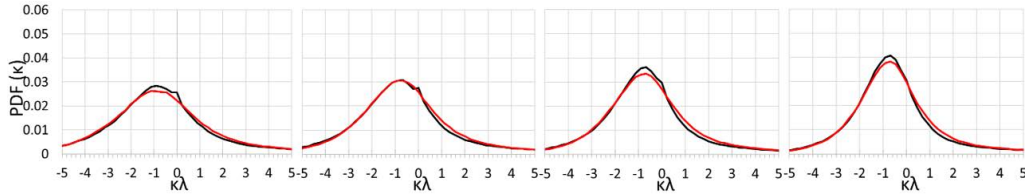


Figure 5. PDF of interfacial curvature at $t/t_L = 0.25, 0.5, 0.75,$ and 1 for $s_L/u' = 0.85$ from DNS (black) and LES-DNS with SDF prolongation (red).

standard gradient-based prolongation operator. This clearly results in a significant under-prediction of the kinetic energy of eddies of size smaller than the initial LES scale mesh. In the actual simulation, a fluid parcel originating on the LES scale mesh does not refine immediately to the DNS scale to interact with the interface but instead has a characteristic residence time on each intermediate mesh level Δx that scales as $\alpha \Delta x / s_L$. However, this time is insufficient to fill in the kinetic energy spectrum on the newly resolved scales, resulting in the observed under-prediction of high curvature probability. Note that increasing the residence time by increasing α is not viable, since it makes the AMR LES-DNS approach prohibitively expensive due to the significant increase in the number of mesh cells.

5.4. LES-DNS with SDF prolongation operator

Figure 5 shows the PDF of curvature obtained at different times from LES-DNS using the proposed SDF prolongation operator. Agreement with the DNS results is excellent and significantly better than the standard prolongation operator, especially on the concave side (gas penetrating the liquid). However, there is a slight over-prediction of the probability of finding intermediate convex curvatures. A potential explanation for this observation lies in the kinetic energy spectrum of the SDF prolongation operator shown in Figure 4. Unlike the standard prolongation operator that significantly under-predicts the kinetic energy of small-scale eddies, the SDF approach with $\mathcal{C} = 0.63$ reconstructs a $-5/3$ spectrum without the viscous subrange of the DNS. However, the aforementioned residence time on intermediate mesh levels is apparently long enough to dissipate at least some of the excess energy at high wave numbers. Furthermore, Huygen's principle may explain why the agreement on the convex side is better than on the concave side.

6. Conclusions

Prior findings from the literature for single-phase flows and the present study of an initially planar normal-propagating phase interface subjected to HIT suggest that aggressive AMR strategies for LES-DNS of turbulent phase interfaces do not self-generate realistic, fully resolved velocities. The standard gradient-based AMR prolongation operator under-predicts the probability of high curvature regions of the interface compared to reference DNS results. This is due to a lack of small-scale eddies responsible for high wave number corrugations of the interface. A new SDF prolongation operator is proposed that uses a spectral enrichment procedure that involves approximate deconvolution and reconstruction of newly resolvable fluctuations. Using the new SDF operator, excellent agreement with reference DNS results of the interface curvature statistics is achieved. Future work will focus on the momentum transport through mesh refinement boundaries. It is likely that a similar enrichment procedure to the SDF prolongation operator

is necessary when, unlike in the case studied here, there is on average notable transport through those mesh refinement boundaries.

Acknowledgments

The authors acknowledge use of computational resources from the Yellowstone cluster awarded by the National Science Foundation to CTR.

REFERENCES

- ANISZEWSKI, W. 2016 Improvements, testing and development of the ADM-tau sub-grid surface tension model for two-phase LES. *J. Comput. Phys.* **327**, 389–415.
- BALLESTEROS, C. 2019 A parallel adaptive mesh refinement library for cartesian meshes. *PhD Thesis*, Arizona State University.
- BASSENNE, M., ESMAILY, M., LIVESCU, D., MOIN, P. & URZAY, J. 2019 A dynamic spectrally enriched subgrid-scale model for preferential concentration in particle-laden turbulence. *Int. J. Multiphase Flow* **116**, 270–280.
- CHANG, J., HE, L., CHEN, L., SHEN, Z., CHUAH, L. F., BOKHARI, A., KLEMES, J. J. & HAN, N. 2022 Numerical simulation of liquid jet atomization in subsonic crossflow. *Energy* **257**, 124676.
- CHESNEL, J., REVEILLON, J., MENARD, T. & DEMOULIN, F. 2011 Subgrid analysis of liquid jet atomization. *Atom. Sprays* **21**, 41–67.
- CHIODI, R. & DESJARDINS, O. 2017 DNS of turbulent phase interfaces. *Private Communication*.
- COOK, A. W. 1999 A consistent approach to large eddy simulation using adaptive mesh refinement. *J. Comput. Phys.* **154**, 117–133.
- GERMANO, M., PIOMELLI, U., MOIN, P. & CABOT, W.H. 1991 A dynamic subgrid-scale eddy viscosity model. *Phys. Fluids* **3**, 1760–1765.
- GOODRICH, A., KEDELTY, D. & HERRMANN, M. 2022 A dual-scale sub-grid closure for LES of phase interfaces with phase change. *Proceedings of the Summer Program*, Center for Turbulence Research, Stanford University, pp. 205–214.
- GROSSHANS, H. 2013 Large Eddy Simulation of Atomizing Sprays. *PhD Thesis*, Lund University.
- HASSLBERGER, J., KETTERL, S., & KLEIN, M. 2020 A-Priori Assessment of Interfacial Sub-grid Scale Closures in the Two-Phase Flow LES Context. *Flow, Turbul. Combust.* **105**, 359–375.
- HERRMANN, M. 2008 A balanced force refined level set grid method for two-phase flows on unstructured flow solver grids. *J. Comput. Phys.* **227**, 2674–2706.
- HERRMANN, M. & GOROKHOVSKI, M. 2008 An outline of a LES subgrid model for liquid/gas phase interface dynamics. *Proceedings of the Summer Program*, Center for Turbulence Research, Stanford University, pp. 171–181.
- HERRMANN, M., KEDELTY, D. & ZIEGENHEIN, T. 2018 A dual-scale subgrid closure for LES of phase interfaces in turbulent flows. *Proceedings of the Summer Program*, Center for Turbulence Research, Stanford University, pp. 45–54.
- HINZE, J. 1955 Fundamentals of the hydrodynamic mechanism of splitting in dispersion processes. *AIChE* **1**, 289–295.
- KOLMOGOROV, A. 1949 On the breakage of drops in a turbulent flow. *Doklady Akademii Nauk SSSR* **66**, 825–828.

- KRAVCHENKO, A., MOIN, P. & MOSER, R. 1996 Zonal embedded grids for numerical simulations of wall-bounded turbulent flows. *J. Comput. Phys.* **127**, 412–423.
- KUO, C. W. & TRUJILLO, M. F. 2018 Benefits of AMR for atomization calculations. *ICLASS Paper 2018*.
- LABOURASSE, E., LACANETTE, D., TOUTANT, A., LUBIN, P., VINCENT, S., LEBAGUE, O., CALTAGIRON, J. P. & SAGAUT, P. 2007 Towards large eddy simulation of isothermal two-phase flows: Governing equations and a priori tests. *Int. J. Multiphase Flow* **33**, 1–39.
- LI, X. & SOTERIOU, M. C. 2018 Detailed numerical simulation of liquid jet atomization in crossflow of increasing density. *Int. J. Multiphase Flow* **104**, 214–232.
- LIOVIC, P. & LAKEHAL, D. 2012 Subgrid-scale modelling of surface tension within interface tracking-based Large Eddy and Interface Simulation of 3D interfacial flows. *Comput. Fluids* **63**, 27–46.
- MARMOTTANT, P. & VILLERMAUX, E. 2004 On spray formation. *J. Fluid Mech.* **498**, 73–111.
- MELLER, R., SCHLEGEL, F. & KLEIN, M. 2022 Sub-grid scale modeling and a-posteriori tests with a morphology adaptive multifield two-fluid model considering rising gas bubbles. *Flow. Turb. Combust.* **108**, 895–922.
- OWKES, M. & DESJARDINS, O. 2014 A computational framework for conservative, three-dimensional, unsplit, geometric transport with application to the volume-of-fluid (VOF) method. *J. Comput. Phys.* **270**, 587–612.
- PETERS, N. 1992 A spectral closure for premixed turbulent combustion in the flamelet regime. *J. Fluid Mech.* **242**, 611–629.
- PIOMELLI, U., KANG, S., HAM F. & IACCARINO, G. 2006 Effect of discontinuous filter width in large-eddy simulations of plane channel flow. *Proceedings of the Summer Program*, Center for Turbulence Research, Stanford University, pp. 171–181.
- POPINET, S. 2003 Gerris: a tree-based adaptive solver for the incompressible Euler equations in complex geometries. *J. Comput. Phys.* **190**, 572–600.
- POPINET, S. 2009 An accurate adaptive solver for surface tension-driven interfacial flows. *J. Comput. Phys.* **228**, 5838–5866.
- SAEEDIPOUR, M. & SCHNEIDERBAUER, S. 2021 Favre-filtered LES-VOF of two-phase flows with eddy viscosity-based subgrid closure models: An a-posteriori analysis. *Int. J. Multiphase Flow* **144**, 103780.
- SHIRANI, E., GHADIRI, F. & AHMADI, A. 2011 Modeling and simulation of interfacial turbulent flows. *J. Appl. Fluid Mech.* **4**, 43–49.
- TOUTANT, A., LABOURASSE, E., LEBAGUE, O. & SIMONIN, O. 2008 DNS of the interaction between a deformable buoyant bubble and a spatially decaying turbulence: A priori tests for LES two-phase flow modelling. *Comput. Fluids* **37**, 877–886.
- VANELLA, M., PIOMELLI, U. & BALARAS, E. 2008 Effect of grid discontinuities on large-eddy simulation statistics and flow fields. *J. Turbu.* **9**, N32.
- ZANDIAN, A., SIRIGNANO, W. A. & HUSSAIN, F. 2019 Length-scale cascade and spread rate of atomizing planar liquid jets. *Int. J. Multiphase Flow* **113**, 117–141.
- ZHANG, B., POPINET, S. & LING, Y. 2020 Modeling and detailed numerical simulation of the primary breakup of a gasoline surrogate jet under non-evaporative operating conditions. *Int. J. Multiphase Flow* **130**, 103362.